

Intrinsic transverse relaxation mechanisms of polarized alkali atoms enclosed in radio-frequency magnetometer cell

Yang-Ying Fu(傅杨颖), Jie Yuan(袁杰)
Citation: Chin. Phys. B . 2019, 28(9): 098504 . **doi:** 10.1088/1674-1056/28/9/098504
Journal homepage: http://cpb.iphy.ac.cn; http://iopscience.iop.org/cpb

What follows is a list of articles you may be interested in

Influence factor analysis of field-free molecular orientation

Jing-Song Liu(刘劲松), Qi-Yuan Cheng(程起元), Da-Guang Yue(岳大光), Xu-Cong Zhou(周旭聪), Qing-Tian Meng(孟庆田)
Chin. Phys. B . 2018, 27(3): 033301 . **doi:** 10.1088/1674-1056/27/3/033301

Numerical analyses on optical limiting performances of chloroindium phthalocyanines with different substituent positions

Yu-Jin Zhang(张玉瑾), Xing-Zhe Li(李兴哲), Ji-Cai Liu(刘纪彩), Chuan-Kui Wang(王传奎)
Chin. Phys. B . 2016, 25(1): 013302 . **doi:** 10.1088/1674-1056/25/1/013302

Photon pair source via two coupling single quantum emitters

Peng Yong-Gang, Zheng Yu-Jun
Chin. Phys. B . 2015, 24(10): 104206 . **doi:** 10.1088/1674-1056/24/10/104206

Interferences in photo-detached electron spectra froma non-collinear tri-atomic anion

A. Afaq, K. Farooq, M. A. Khan, Yi Xue-Xi
Chin. Phys. B . 2014, 23(10): 103304 . **doi:** 10.1088/1674-1056/23/10/103304

Field-free molecular orientation induced by combined femtosecond single- and dual-color laser pulses：The role of delay time and quantum interference

Qin Chao-Chao, Jia Guang-Rui, Zhang Xian-Zhou, Liu Yu-Fang, Long Jin-You, Zhang Bing
Chin. Phys. B . 2014, 23(1): 013302 . **doi:** 10.1088/1674-1056/23/1/013302

Intrinsic transverse relaxation mechanisms of polarized alkali atoms enclosed in radio-frequency magnetometer cell*

Yang-Ying Fu(傅杨颖) and Jie Yuan(袁杰)†

College of Advanced Interdisciplinary Studies, National University of Defense Technology, Changsha 410073, *China*

(Received 15 April 2019; revised manuscript received 2 July 2019; published online 20 August 2019)

The intrinsic transverse relaxation mechanisms of polarized alkali atoms enclosed in the radio-frequency magnetometer cell are investigated. The intrinsic transverse relaxation rate of cesium atoms as a function of cell temperature is obtained. The absorption of alkali atoms by the glass wall and the reservoir effect are the main error factors which contribute to the disagreements between theory and experiments. A modified relaxation model is presented, in which both the absorption of alkali atoms by the glass wall and the reservoir effect are included. This study provides a more accurate description of the intrinsic transverse relaxation mechanisms of polarized alkali atoms, and enlightens the optimization of the cell design.

Keywords: intrinsic transverse relaxation, modified relaxation model, absorption of alkali atoms, reservoir effect

PACS: 85.70.Sq, 42.62.Be, 33.80.–b **DOI:** 10.1088/1674-1056/ab3442

1. Introduction

Due to numerous technological advancements, atomic magnetometers have become an appealing option for magnetic field detection and measurement. The present-day interest in atomic magnetometer is driven by various applications, such as the measurements of the fundamental physics,[1] the detections of biological magnetic fields of the brain (magnetoencephalography (MEG)) and the heart (magnetocadiography (MCG)),[2,3] the tests of nuclear magnetic resonance (NMR) signal,[4] and the attempts at earthquake prediction.[5] Besides, the recent breakthroughs on the size and sensitivity of the atomic magnetometer facilitate the application in space exploration.[6]

For an atomic magnetometer, a resonance excitation is applied to drive most of the alkali atoms to precess together with a uniform phase. Two techniques are commonly used for the resonance excitation, namely, radio-frequency excitation[7–9] and optical excitation.[10–13] Numerous high-sensitive atomic magnetometers have been developed in recent years, among all these magnetometers, the self-exchange-relaxation-free (SERF) magnetometer is the most sensitive one.[14–17] Despite of all these advancements, the key parts of these devices remain unchanged, a glass cell containing spin-polarized alkali vapor is typically applied as the magnetic field sensor. The atomic magnetometer is generally characterized by the field sensitivity, which represents the precision of the magnetic field measurement in one second of integration. Considerable attention has been paid to the enhancement of the magnetometer sensitivity, and the most effective way is to maximize the spin relaxation time of alkali atoms. Since the alkali atoms can be depolarized by diverse mechanisms, steps should be taken to suppress the spin relaxation. Two methods are commonly applied to suppress the relaxation due to wall collisions, one is the introduction of buffer gas into the cell,[18–21] the other one is the use of antirelaxation coatings.[22–26] The relaxation due to spin-exchange collisions can be completely eliminated through operating in the spin-exchange-relaxation-free (SERF) regime, or partially suppressed by light narrowing.[27–29] The depolarization produced by the magnetic field gradient across the cell can be avoided through compensation techniques.[30–32]

In order to mitigate the spin relaxation due to wall collisions, buffer gas and quenching gas are introduced into the atomic cells. In this paper, experimental measurements are carried out in a cesium atomic radio-frequency magnetometer. Through eliminating the depolarization due to power broadening, radio-frequency magnetic field, and magnetic-field gradient, the intrinsic transverse relaxation rate of cesium atoms is obtained. The error factors which result in the disagreements between theory and experiments are studied. A modified relaxation model is consequently given, which provides a more reasonable explanation for the intrinsic transverse relaxation mechanisms of polarized alkali atoms enclosed in the magnetometer cell.

2. Theory model

The alkali atoms enclosed in the magnetometer cell can be depolarized by diverse processes, including collisions with the glass wall, buffer gas atoms, quenching gas molecules, and other alkali atoms. Additionally, the magnetic-field gradient across cell, optical pumping, absorption of probe light, and the radio-frequency (RF) magnetic field will also produce relax-

*Project supported by the National Natural Science Foundation of China (Grant No. 61475192).

†Corresponding author. E-mail: jieyuan@nudt.cn

© 2019 Chinese Physical Society and IOP Publishing Ltd

ation. In this paper, the spin relaxation due to optical pumping and the absorption of the probe light is referred to as power broadening relaxation. In order to enhance the magnetometer sensitivity, the relaxation rate of alkali atoms, which is the inverse of the relaxation time, should be minimized.

Any process which affects the expectation value of the longitudinal spin polarization component contributes to the longitudinal relaxation rate. The longitudinal relaxation rate is thus given by

$$\Gamma_1 = \frac{1}{q}\left(R_{\rm SD} + R_{\rm OP} + R_{\rm probe}\right) + R_{\rm wall}, \tag{1}$$

where $R_{\rm SD}$, $R_{\rm wall}$, and $R_{\rm probe}$ denote the relaxation rates due to spin-destruction collisions, wall collisions, and the absorption of the probe light, respectively, and $R_{\rm OP}$ denotes the optical pumping rate, which is proportional to the pump power $I_{\rm pump}$, i.e., $R_{\rm OP} = \alpha I_{\rm pump}$. In this paper, the scale factor α (see Appendix A) is considered to be constant. Since the nuclear spin of alkali atoms will not be destroyed by the term in the parentheses of Eq. (1), a nuclear slowing-down factor q is thus introduced, which describes the degree to which the spin coherence is maintained. In addition, the nuclear slowing-down factor is spin polarization dependent. The total effect of these processes is to randomize the spin direction of alkali atoms, and drive the longitudinal polarization component toward the thermal equilibrium value.

The mechanisms that cause the dephasing of the processing atoms generate the transverse relaxation of alkali atoms. Consequently, one obtains the transverse relaxation rate

$$\Gamma_2 = \Gamma_1 + \frac{1}{q_{\rm SE}} R_{\rm SE} + R_{\nabla B} + R_{\rm RF}, \tag{2}$$

where $R_{\rm SE}$, $R_{\nabla B}$, and $R_{\rm RF}$ denote the rates of depolarization due to spin-exchange collisions, magnetic-field gradient, and the RF magnetic field, respectively, and $q_{\rm SE}$ denotes the spin-exchange broadening factor, which depends on the magnitude of the ambient magnetic field and the alkali vapor density. In a strong magnetic field, where the precession frequency of alkali atoms $\omega_{\rm L}$ is much larger than the spin-exchange collisions rate $R_{\rm SE}$, the spin-exchange broadening factor follows

$$\frac{1}{q_{\rm SE}} = \frac{2I(2I-1)}{3(2I+1)^2}, \tag{3}$$

where I is the nuclear spin quantum number of alkali atoms, for ^{133}Cs, $I = 7/2$. In our experiments, the condition $\omega_{\rm L} \gg R_{\rm SE}$ is satisfied, the spin-exchange broadening factor is thus $1/q_{\rm SE} = 7/32$.

Generally, the atomic magnetometer monitors the spin coherence of the precessing atoms, so special attention is paid to the transverse relaxation mechanisms of alkali atoms. In this paper, the intrinsic relaxation mechanisms of cesium atoms are investigated. The intrinsic relaxation refers to the depolarization which only depends on the cell design and temperature. Therefore, the relaxation due to power broadening, magnetic-field gradient, and RF magnetic field should not be included. For a spherical cell, the intrinsic transverse relaxation rate of alkali atoms Γ_{20} is then given by

$$\begin{aligned}\Gamma_{20} &= \frac{1}{q}R_{\rm SD} + R_{\rm wall} + \frac{1}{q_{\rm SE}}R_{\rm SE} \\ &= \frac{1}{q}\left(n_{\rm B}\overline{v}_{\rm A-B}\sigma_{\rm SD}^{\rm A-B} + n_{\rm Q}\overline{v}_{\rm A-Q}\sigma_{\rm SD}^{\rm A-Q} + n_{\rm A}\overline{v}\sigma_{\rm SD}^{\rm A-A}\right) \\ &\quad + D\frac{P_0}{P_{\rm B}(T)}\left(\frac{\pi}{r}\right)^2 + \frac{1}{q_{\rm SE}}n_{\rm A}\overline{v}\sigma_{\rm SE}^{\rm A-A},\end{aligned} \tag{4}$$

where $n_{\rm B}$, $n_{\rm Q}$, and $n_{\rm A}$ denote the densities of buffer gas, quenching gas, and alkali atoms, respectively. Quenching gas, typically nitrogen, is introduced into the cell to suppress the problem of radiation trapping.[33] $\overline{v}_{\rm A-B,Q}$ denotes the relative thermal velocity between the alkali atoms and buffer gas or quenching gas, and $\overline{v}$ denotes the average thermal velocity of the alkali atoms. $\sigma_{\rm SD}$ and $\sigma_{\rm SE}$ denote the cross sections of spin-destruction collisions and spin-exchange collisions, respectively. Equation (4) indicates that the depolarization due to wall collisions depends on the cell radius r, the cell temperature T, and the diffusion constant of alkali atoms in buffer gas D. P_0 is the standard atmospheric pressure, and $P_{\rm B}(T)$ denotes the buffer gas pressure at temperature T. Generally, the spin-destruction collision cross section is two orders of magnitude smaller than the spin-exchange one. Therefore, for a high-density atomic cell, the depolarization due to the spin-exchange collisions dominates. For a specific cell, the intrinsic transverse relaxation rate at any cell temperature can be inferred according to Eq. (4).

3. Experiments and discussion

Figure 1 shows the schematic diagram of the experimental setup, the cesium atomic radio-frequency magnetometer is the same as the one described in Ref. [27]. The heating and temperature control unit is composed of three components, including electric heating films, a fixture, and a thermistor. The fixture, which is made of non-magnetic thermal conductive material, is used to hold the Cs cell in place. The alternating-current heating approach is applied in our experiments, and the electric heating films are fixed at the surfaces of the fixture to vaporize the cesium atoms enclosed in the cell. The thermistor is utilized to measure and stabilize the cell temperature through a feedback controlling program. The three-axis coils are utilized to generate the simulated magnetic field, including the static bias magnetic field, the RF magnetic field, and the gradient magnetic field. All these elements are placed in the center of a five-layer magnetic-shield cylinder. The pump light, parallel to the bias magnetic field, is applied to polarize the ensemble of cesium atoms. The coherent spin precession of cesium atoms is probed with a linearly polarized probe light propagating orthogonally to the bias magnetic field. The optical rotation signal of the probe light is then detected by the balanced polarimetry technique. The pump and probe power can be adjusted by the attenuators.

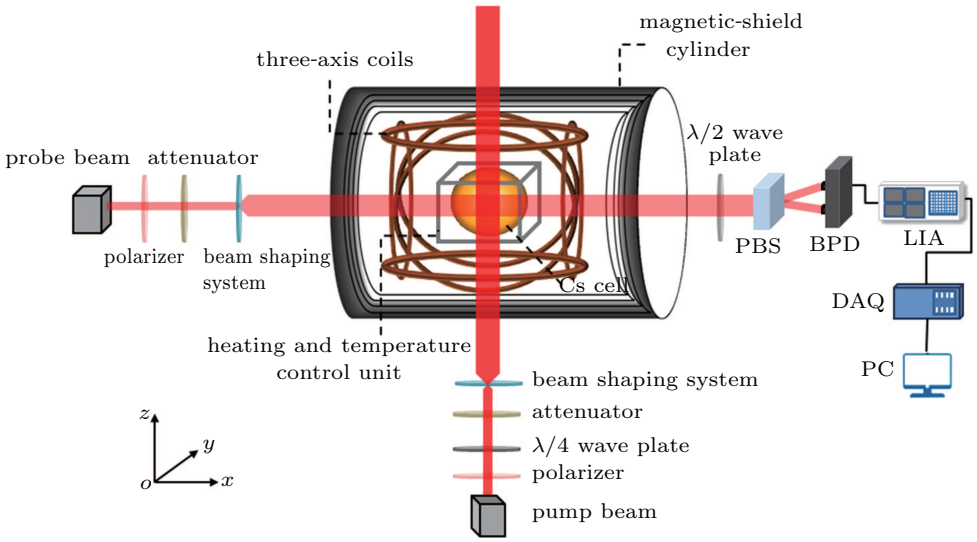


Fig. 1. Sketch of the experimental setup of cesium atomic radio-frequency magnetometer. PBS: polarization beam splitter, BPD: balanced photodetector, LIA: lock-in amplifier, DAQ: data acquisition card, PC: personal computer.

The transverse relaxation rates of cesium atoms are obtained through the free-induction decay method.[34] The measured transverse rates are the total ones, which contain the contributions from the intrinsic relaxation, power-broadening, magnetic field gradient, and RF magnetic field. In order to get the intrinsic transverse relaxation rate of cesium atoms, the depolarization due to power broadening, magnetic-field gradient, and RF magnetic field should be eliminated. In our experiments, a waveform generator is connected to the RF coils to produce the RF magnetic field. In addition, the RF magnetic field intensity is proportional to the amplitude of the sinusoidal signal produced by the waveform generator. In order to obtain the depolarization due to the RF magnetic field, the impact of the RF magnetic field on the cesium magnetic-resonance linewidth is investigated. In our experiments, the RF magnetic field is characterized by the peak-to-peak voltage of the output sinusoidal signal, which is referred to as the relative RF amplitude. Figure 2 plots the cesium magnetic-resonance linewidth against the relative RF amplitude. The experimental results show that the square of the linewidth has a quadratic dependence on the relative RF amplitude, which agrees with the theoretical result in Ref. [21]. Under our experimental conditions, the depolarization due to the RF magnetic field can be regarded as perturbation. In addition, the depolarization produced by the magnetic field gradient is obtained through a compensation method. The impact of the longitudinal magnetic field gradient on the transverse relaxation rate of cesium atoms has been studied in Ref. [35]. Under our experimental condition, the relaxation rate due to the magnetic field gradient is about 40 s^{-1}.

Then, the depolarization due to power broadening is investigated. Figure 3 profiles the dependence of the measured transverse relaxation rate on the probe power. The experimental results indicate that, when the cell temperature is in the range from 40 °C to 90 °C, the transverse relaxation rate of cesium atoms increases linearly with the increasing probe power.

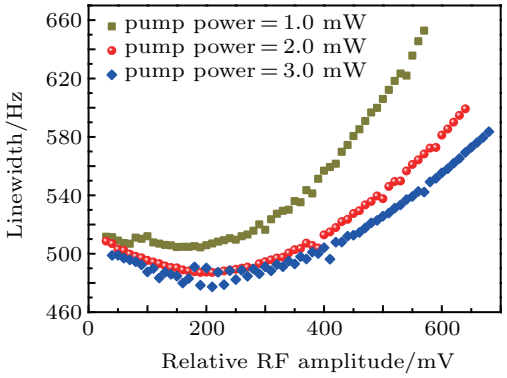


Fig. 2. Dependence of cesium magnetic-resonance linewidth on the relative RF amplitude. The experimental measurements are carried out at $T = 77$ °C with a probe power of 100 μW. The frequency of the pump light is detuned 1.95 GHz from the cesium D1 transition, and the probing frequency is detuned −20.16 GHz from the cesium D2 transition.

Through extrapolating fits, the transverse relaxation rate of cesium atoms at zero probe power is obtained, and the depolarization due to the absorption of the probe light is thus eliminated. Figure 4 shows the measured transverse relaxation rate of cesium atoms as a function of the pump power. As we can see, the impact of the pump power on the transverse relaxation rate of cesium atoms is temperature dependent. In the linear region, as shown in Fig. 4(a), the transverse relaxation rate of cesium atoms increases as the pump power is increased. However, when the cell temperature is higher than 60 °C, as shown in Fig. 4(b), the transverse relaxation rate of cesium atoms will be reduced by enhancing the pump power. Since the results in Fig. 4(b) can be explained by the light narrowing effect, it is referred to as light narrowing region.

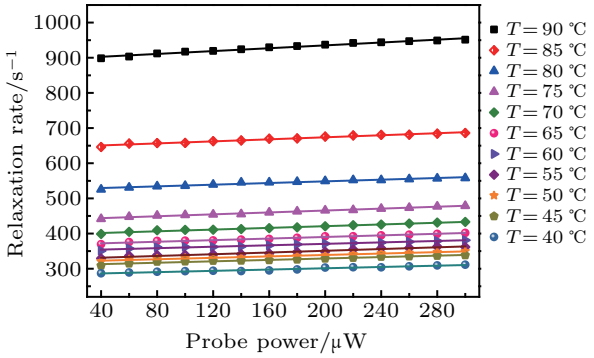


Fig. 3. The measured transverse relaxation rates of cesium atoms as a function of the probe power. The solid lines denote the liner fitting results.

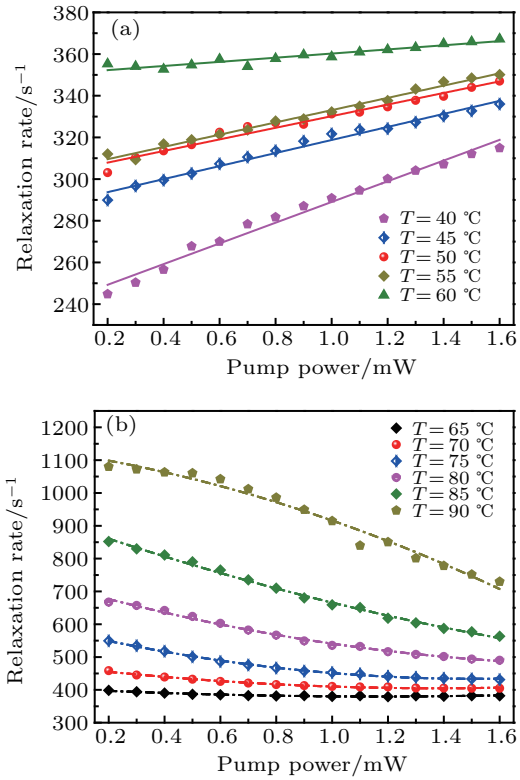


Fig. 4. The measured transverse relaxation rates of cesium atoms as a function of the pump power: (a) linear region, (b) light narrowing region.

For the ground-state transition of cesium atoms, the total linewidth due to optical pumping, spin-destruction collisions, and spin-exchange collisions follows[27]

$$\Delta\nu = \frac{9}{16}R_{\rm SD} + \frac{1}{8}R_{\rm OP} + R_{\rm SE}\left[\frac{9-7P}{16} - \frac{1}{4}\frac{P(1+P)^7}{(1+P)^8-(1-P)^8}\right]. \quad (5)$$

The spin-polarization P is given by

$$P = \frac{R_{\rm OP}}{R_{\rm OP}+R_{\rm rel}}, \quad (6)$$

where $R_{\rm rel}$ denotes the effective relaxation rate of cesium atoms without the contribution from optical pumping. The first term on the right side of Eq. (5) describes the linewidth broadening due to the spin-destruction collisions. The second term denotes the linewidth produced by optical pumping, and the last term characterizes the linewidth broadening arised from the spin-exchange collisions. Through enhancing the pump power, the term in the square brackets will be decreased, and the linewidth due to the spin-exchange collisions will be narrowed. This effect is attributed to the partially suppression of Cs–Cs spin-exchange relaxation. For a high-temperature atomic cell, the relaxation rate due to the spin-exchange collisions is much larger than the one caused by optical pumping and spin-destruction collisions. Consequently, the reduction of linewidth will occur. The effect that the total linewidth decreases with the rising pump power is referred to as light narrowing. In addition, the transverse relaxation rate of cesium atoms scales linearly with the total linewidth, thus the results in Fig. 4(b) can be explained with the light narrowing effect.

The intrinsic transverse relaxation rates of cesium atoms are thus obtained through eliminating the depolarization due to power broadening, magnetic-field gradient, and RF magnetic field. The intrinsic transverse relaxation rate of cesium atoms as a function of the cell temperature is plotted in Fig. 5. The results, both experimental and theoretical ones, indicate that the intrinsic transverse relaxation rate of cesium atoms increases significantly with the rising cell temperature. In the following text, further attention is paid to the factors which lead to the disagreements between the theoretical and experimental results.

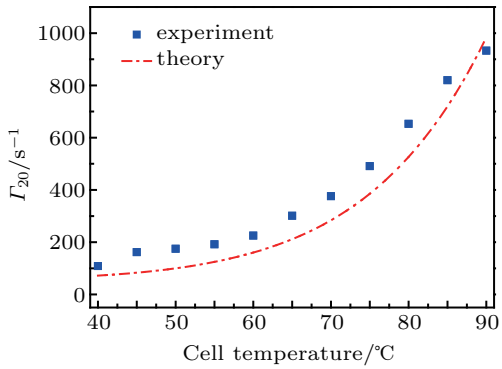


Fig. 5. The dependence of intrinsic transverse relaxation rate on the cell temperature. The experimental measured results are denoted by blocks, and the theory values given by Eq. (4) are denoted by the dash-line.

During the heating process, cesium atoms vapor will be absorbed by the glass wall, which reduces the cesium atoms density. In this paper, the real cesium atoms density is obtained through the absorption approach.[18,19] The experimental results show that the real cesium atoms density is typically 15%–50% smaller than the theoretical one, which indicates that the absorption of cesium atoms by the glass wall is about 15%–50%. Additionally, the absorption of cesium atoms will be enhanced as the cell temperature is increased. Since the relaxation rates due to spin-destruction collisions and spin-exchange collisions are both cesium atoms density dependent, the intrinsic transverse relaxation rate of cesium atoms will be

reduced by the absorption of cesium atoms. Nevertheless, the results in Fig. 5 suggest that the measured intrinsic transverse relaxation rates are generally larger than the values predicted by Eq. (4). Therefore, there should be another error factor which enlarges the intrinsic transverse relaxation rate of cesium atoms.

The Cs cell applied in our experiments is composed of two parts, namely, the spherical bulb and the sidearm. The spherical bulb serves as the active region, and the sidearm is used to hold the droplet of the solid cesium. During heating, the cesium atoms in the active region can escape to the sidearm and collide with the glass wall and solid cesium droplet. Collisions and exchanges of cesium atoms between the active region and the sidearm can produce rapid depolarization, which increases the intrinsic transverse relaxation rate of cesium atoms. The depolarization due to the sidearm is generally called the reservoir effect. In Ref. [30], the relaxation rate produced by the reservoir effect is estimated as the probability of an alkali atom hitting the sidearm after it has bounced off the glass wall. However, there has not been a general model of the reservoir effect.[36,37] In both laboratory researches and engineering applications, the reservoir effect is commonly suppressed with special techniques. By constricting the sidearm close to the active region into a capillary,[36] the exchanges and collisions of alkali atoms between these two parts can be suppressed. A coated lockable stem can also be applied,[38] which reduces the depolarization rate due to wall collisions. Additionally, through adjusting the position of the lockable stem, the collision and exchange rate of alkali atoms between the active region and the sidearm can be reduced.

Finally, a modified relaxation model is presented, in which both the absorption of alkali atoms by the glass wall and the reservoir effect are included,

$$\begin{aligned}\Gamma_{20} &= \frac{1}{q}R_{\mathrm{SD}}+R_{\mathrm{wall}}+\frac{1}{q_{\mathrm{SE}}}R_{\mathrm{SE}}+R_{\mathrm{res}}\\ &= \frac{1}{q}\left(n_{\mathrm{B}}\overline{v}_{\mathrm{A-B}}\sigma_{\mathrm{SD}}^{\mathrm{A-B}}+n_{\mathrm{Q}}\overline{v}_{\mathrm{A-Q}}\sigma_{\mathrm{SD}}^{\mathrm{A-Q}}\right.\\ &\quad\left.+\left(n_{\mathrm{A}}-\delta n_{\mathrm{A}}\right)\overline{v}\sigma_{\mathrm{SD}}^{\mathrm{A-A}}\right)+D\frac{P_0}{P_{\mathrm{B}}(T)}\left(\frac{\pi}{r}\right)^2\\ &\quad+\frac{1}{q_{\mathrm{SE}}}\left(n_{\mathrm{A}}-\delta n_{\mathrm{A}}\right)\overline{v}\sigma_{\mathrm{SE}}^{\mathrm{A-A}}+R_{\mathrm{res}},\end{aligned}\tag{7}$$

where R_{res} denotes the relaxation rate due to the reservoir effect, and δn_{A} denotes the absorption of alkali atoms by the glass wall, which is generally temperature dependent. In our experiments, δn_{A} is 15%–50% of n_{A}. For a specific cell and temperature, the absorption of alkali atoms by the glass wall is not invariable. Therefore, the value of δn_{A} should be obtained through experimental measurements. Ongoing work is focused on the establishment of the theory model of the reservoir effect, which benefits the accurate explanation of the intrinsic relaxation mechanisms of alkali atoms. Moreover, more attention should be paid to the optimization of the cell design to suppress the the reservoir effect.

4. Conclusion

We have studied the intrinsic transverse relaxation mechanisms of polarized alkali atoms enclosed in the magnetometer cell. The intrinsic transverse relaxation rate of cesium atoms as a function of the cell temperature is obtained. The disagreements between theory and experiments are mainly attributed to the absorption of cesium atoms by the glass wall and the reservoir effect. In future works, special attention needs to be paid to the suppression of the reservoir effect. Although the relaxation rate due to the reservoir effect is not given in this paper, a general model of the reservoir effect should be established to provide a more accurate description of the intrinsic transverse relaxation mechanisms of polarized alkali atoms.

Appendix A

The optical pumping rate is proportional to the pump power, with $R_{\mathrm{OP}}=\alpha I_{\mathrm{pump}}$. The scale factor α is referred to as the optical-pumping rate constant, which is independent of the pump power, and is given by

$$\alpha=\frac{2\sqrt{\pi\ln 2}r_{\mathrm{e}}f\lambda^3 w'(r,s)}{hc\delta\lambda A},$$

where r_{e} denotes the classical electron radius, c denotes the speed of light, f denotes the oscillator strength of the optical transition, h is the Planck constant, λ is the wavelength of the pump light, A is the effective pump area, and $\delta\lambda$ is the full width at half maximum (FWHM) of the pump light. w' denotes the real part of the complex overlap function w, which follows

$$w=w'+\mathrm{i}w''=\exp\left[\ln 2\,(r+\mathrm{i}s)^2\right]\mathrm{erfc}\left(\sqrt{\ln 2}[r+\mathrm{i}s]\right),$$

where s is the relative detuning, $s=2(\nu_{\mathrm{l}}-\nu_{\mathrm{a}})/\delta\nu_{\mathrm{l}}$, r is the relative linewidth, $r=\delta\nu_{\mathrm{a}}/\delta\nu_{\mathrm{l}}$, and erfc is the Gaussian error function. For the D1 line transition of cesium atoms, the oscillator strength is about $1/3$.

Acknowledgment

We would like to thank Beijing Vacuum Electronic Technology Research for the technical support.

References

[1] Bear D, Stoner R E and Walsworth R L 2002 *Phys. Rev. Lett.* **89** 209902
[2] Savukov I M, Seltzer S J and Romalis M V 2007 *J. Magn. Reson* **185** 214
[3] Savukov I M and Romalis M V 2005 *Phys. Rev. Lett.* **94** 123001
[4] Liu G, Li X and Sun X 2013 *J. Magn. Reson.* **237** 158
[5] Balasis G, Mandea M 2007 *Tectonophysics* **431** 1173
[6] Budker D and Romalis M 2007 *Nat. Phys.* **3** 227
[7] Savukov I M and Seltzer S J 2005 *Phys. Rev. Lett.* **95** 063004
[8] Lee S K, Sauer K L and Seltzer S J 2006 *Appl. Phys. Lett.* **89** 214106

[9] Keder D A, Prescott D W and Conovaloff A W 2014 *AIP Adv.* **4** 127159
[10] Zhang J, Lin Q and Zeng X 2012 *Chin. Phys. Lett.* **29** 068501
[11] Pustelny S, Wojciechowski A and Kotyrba M 2007 14*th International School on Quantum Electronics: Laser Physics and Applications* **6604** 660404
[12] Higbie J M, Corsini E and Budker D 2006 *Rev. Sci. Instrum.* **77** 113106
[13] Patton B, Zhivun E and Hovde D C 2014 *Phys. Rev. Lett.* **113** 013001
[14] Allerd J C, Lyman R N and Kornack T W 2002 *Phys. Rev. Lett.* **89** 130801
[15] Kominis I K, Kornack T W and Allred J C 2003 *Nature* **422** 596
[16] Seltzer S J and Romalis M V 2004 *Appl. Phys. Lett.* **85** 4804
[17] Jiménez-Martínez R, Knappe S and Kitching J 2014 *Rev. Sci. Instrum.* **85** 045124
[18] Romalis M V, Miron E and Cates G D 1997 *Phys. Rev. A* **56** 4569
[19] Pitz G A and Perram G P 2008 *Int. Soc. For Opt. Photon.* **7005** 700526
[20] Pitz G A, Wertepny D E and Perram G P 2009 *Phys. Rev. A* **80** 062718
[21] Shi R Y and Wang Y H 2013 *Chin. Phys. B* **22** 100703
[22] Balabas M V and Tretiak O Y 2013 *Quan. Elec.* **43** 1175
[23] Seltzer S J and D J M M 2010 *J. Chem. Phys.* **133** 144703
[24] Corsini E P, Karaulanov T and Balabas M 2013 *Phys. Rev. A* **87** 022901
[25] Seltzer S J and Romalis M V 2009 *J. Appl. Phys.* **106** 114905
[26] Yi Y W, Robinson H G adn Knappe S 2008 *J. Appl. Phys.* **104** 023534
[27] Fu Y, Liu X and Yuan J 2019 *AIP Adv.* **9** 015304
[28] Appelt S, Baranga A B and Young A R 1999 *Phys. Rev. A* **59** 2078
[29] Seltzer S J 2008 *Developments in Alkali-metal Atomic Magnetometry* (Ph. D. Dissertation) (New Jersey: Princeton University)
[30] Cates G D, Schaefer S R and Happer W 1988 *Phys. Rev. A* **37** 2877
[31] Stoller S D, Happer W and Dyson F J 1991 *Phys. Rev. A* **44** 7459
[32] Hasson K C, Cates G D and Lerman K 1990 *Phys. Rev. A* **41** 3672
[33] Franz F A 1968 *Phys. Lett. A* **27** 457
[34] Mirijanian J 2012 *Techniques to Characterize Vapor Cell Performance for a Nuclear-magnetic-resonance Gyroscope* (California: California Polytechnic State University)
[35] Fu Y and Yuan J 2017 *AIP Adv.* **7** 115315
[36] Castagna N, Bison G and Di Domenico G 2009 *Appl. Phys. B* **96** 763
[37] Bouchiat M A and Brossel J 1966 *Phys. Rev.* **147** 41
[38] Balabas M V, Karaulanov T and Ledbetter M P 2010 *Phys. Rev. Lett.* **105** 070801